# Polarization-Dressed Correlation and Anti-Correlation Between Phase-Conjugate Four-Wave Mixing and Fourth-Order Fluorescence

Ruimin Wang, Yang Liu, Kangkang Li, Peng Li, Muhammad Owais, and Yanpeng Zhang

***Abstract*— We report the two- and three-mode correlation of phase-conjugate four-wave mixing and fourth-order fluorescence in $Pr^{3+}$:$Y_2SiO_5$ crystal. The degree of correlation is controlled by changing the position of detecting time and polarization state of pumping field. The switching between correlation and anti-correlation was observed at different positions of detecting time because of the competition between four-wave mixing and fourth-order fluorescence signals. The obvious variation of correlation degree was also observed at different polarization states, which is interpreted by the different Clebsch–Gordan coefficients and the EIT subsystem induced by polarization dressing effect.**

***Index Terms*— (190.4380) Nonlinear optics, four-wave mixing, (260.2510) fluorescence, (270.1670) coherent optical effects.**

## I. Introduction

IT HAS long been known that there exists correlation between the intensity fluctuations recorded at two different photo-detectors illuminated by the same light source [1]. Such correlation photons have important applications in quantum computation, communications and measuring of atmospheric turbulence [2]. Based on atomic coherence, the generated Stokes and anti-Stokes field components in four-wave mixing (FWM) can possess perfect quantum correlation and significantly suppress the quantum noise [3]. At the same time, photon anti-correlations have been observed in FWM and resonance fluorescence experiments [4]–[6]. In recent years, the correlations among multiple fields [7], [8] have attracted considerable attention because a real quantum information network should be composed of many nodes and channels. The high-order intensity correlations of electromagnetic wave have been studied theoretically [9]–[11]. Nevertheless, many technological challenges and fundamental issues remain in multiple-field correlations.

Manuscript received January 24, 2017; revised April 17, 2017; accepted April 18, 2017. Date of publication May 25, 2017; date of current version June 6, 2017. This work was supported in part by the 973 Program under Grant 2012CB921804, in part by the National Natural Science Foundation of China under Grant 11474228, and in part by the Natural Science Foundation of Shaanxi Province under Grant 2016JM1006. *(Corresponding author: Yanpeng Zhang.)*

The authors are with the School of Science, the Key Laboratory for Physical Electronics and Devices of the Ministry of Education and the Shaanxi Key Laboratory of Information Photonic Technique, Xi'an Jiaotong University, Xi'an 710049, China (e-mail: wangrm@mail.xjtu.edu.cn; ypzhang@mail.xjtu.edu.cn).

Color versions of one or more of the figures in this paper are available online at http://ieeexplore.ieee.org.

Digital Object Identifier 10.1109/JQE.2017.2708521

Rare-earth $Pr^{3+}$ doped $Y_2SiO_5$ (Pr:YSO) exhibits obvious advantages for coherent excitation experiment and practical applications. Many progresses related to atomic coherence effects have been reported in Pr:YSO, such as electromagnetically induced transparency (EIT), enhanced FWM [12], [13] and coherent storage [14]. Based on coherence dressing effect, we observed multi-order fluorescence [15] and spontaneous parametric four-wave mixing (SP-FWM) in Pr:YSO [16]. The competition effects [17] between FWM and fluorescence have been investigated. At the same time, we also observed significantly correlation and squeeze effect between stokes and anti-stokes signals generated in FWM [18].

In this paper, we investigate the two- and three-mode correlation among Stokes, anti-Stokes signals and fourth–order fluorescence (FL) in Λ-type and V-type level system of Pr:YSO crystal. The variation of correlation degree and switching between correlation and anti-correlation are observed at different time delay position and polarization state of pumping field.

## II. Experimental Setup

The sample used in current experiment is 0.05% $Pr^{3+}$ doped YSO crystal, which is held at 77 K in a cryostat (CFM-102). Figure 1(a) shows the energy levels chosen in this experiment. The $Pr^{3+}$ ions occupy two nonequivalent cation sites ($Pr^{3+}$(I) and $Pr^{3+}$(II)) in the YSO crystal. The Stark level $\delta_0$ and $\delta_1$ of the ground-state $^3H_4$ and the lowest Stark level $\gamma_0$ ($\gamma_0^*$) of excited-state $^1D_2$ for $Pr^{3+}$(I) ($Pr^{3+}$(II)) are selected to couple with each other. The homonuclear-like Λ-type three-level system is configured as ($|0\rangle$ ($\delta_0$) $\leftrightarrow$ $|1\rangle$ ($\gamma_0$) $\leftrightarrow$ $|3\rangle$ ($\delta_1$)). Due to the dipole-dipole interactions, the coupling between $Pr^{3+}$(I) and $Pr^{3+}$(II) in the YSO crystal can happen, so one can treat these ion pairs as heteronuclear-like molecules. Hence, a heteronuclear-like V-type three-level system ($|0\rangle$ ($\delta_0$) $\leftrightarrow$ $|1\rangle$ ($\gamma_0$) $\leftrightarrow$ $|2\rangle$ ($\gamma_0^*$)) can be made up.

Figure 1(b) shows the schematic diagram of the experimental arrangement. Three tunable dye lasers (narrow scan with a 0.04 $cm^{-1}$ linewidth) pumped by an injection locked single-mode Nd:YAG laser (Continuum Powerlite DLS 9010, 10 Hz repetition rate, 5 ns pulse width) are used to generate the pumping fields $\boldsymbol{E}_1$ ($\omega_1$, $\Delta_1$), $\boldsymbol{E}_2$ ($\omega_2$, $\Delta_2$), and $\boldsymbol{E}_3$ ($\omega_3$, $\Delta_3$) with the frequency detuning of $\Delta_i$ ($i = 1, 2, 3$), respectively. $\boldsymbol{E}_1$ drives the transition $|0\rangle$ ($\delta_0$) $\leftrightarrow$ $|1\rangle$ ($\gamma_0$), $\boldsymbol{E}_2$ ($\boldsymbol{E}_3$) couples to the transition $|0\rangle$ ($\delta_0$) $\leftrightarrow$ $|2\rangle$ ($\gamma_0^*$) ($|1\rangle$($\gamma_0$) $\leftrightarrow$ $|3\rangle$($\delta_1$)). Two strong beams $\boldsymbol{E}_1$ and $\boldsymbol{E}_2$ (or $\boldsymbol{E}_3$)

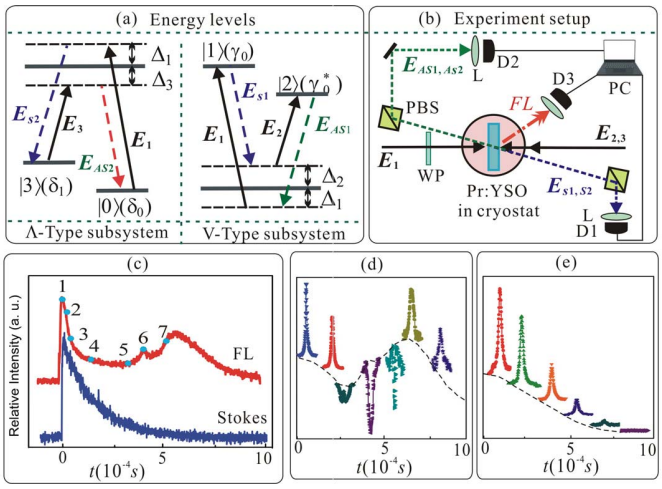


Fig. 1. (color online). (a) Λ-type and V-type three-level system in Pr:YSO. (b) Experimental setup. PBS: polarized beam splitter, WP: wave-plate, and L: lens. (c) Fluorescence and Stokes signals in time domain. (d) Fluorescence and (e) Stokes spectra detected at different delay time, respectively.

counter-propagate through the YSO crystal, the generated Stokes $\boldsymbol{E_S}$ and anti-Stokes $\boldsymbol{E_{AS}}$ signals satisfy the phase-matching condition $\mathbf{k}_1 + \mathbf{k}_{2,3} = \mathbf{k}_{S1} + \mathbf{k}_{AS2,3}$. The vertically polarized components (S-polarization) of Stokes and anti-Stokes signals reflected by PBS are detected by two photomultiplier tubes (D1 and D2). The half-wave-plate (HWP) and quarter-wave-plate (QWP) are used to control the polarization states of pumping field $\boldsymbol{E}_1$. Simultaneously, a composite signal (including FL and SP-FWM) are monitored by another photomultiplier tube D3 with a fast boxcar gated integrator. The signals from detectors were processed by the PC to obtain the intensity noise correlation function. Figure 1(c) shows the FL and Stokes signals in time domain. There exist two peaks in FL spectrum. The reason is that particles are excited to $|1\rangle$ which is split into $|G_1\pm\rangle$ caused by $\boldsymbol{E}_1$. In addition, $\boldsymbol{E}_2$ further splits $|G_{1+}\rangle$ into $|G_{2+\pm}\rangle$. The obvious delay of the right peak in FL spectrum is caused by the residual particles in $|G_{2++}\rangle$ transferring to $|G_{1-}\rangle$ through phonon-assisted nonradioactive transition. The Stokes spectrum $\boldsymbol{E_S}$ has a single peak because it is insensitive to dressing effect. Figures 1(d) and (e) show the FL and $\boldsymbol{E_S}$ spectra detected at different delay time. We get spectral signals by scanning frequency detuning $\Delta_1$ and temporal signals by fixing $\Delta_1 = 0$.

## III. Theoretical Model

### A. The Polarization-Dressed Phase-Conjugate Four-Wave Mixing

The intensity of FWM is proportional to the third-order nonlinear density matrix elements. For V-type three-level system taking into account the self-dressing effect of $\boldsymbol{E}_1$ and the external-dressing effect of $\boldsymbol{E}_2$, the third-order nonlinear density matrix elements of $\boldsymbol{E}_{S1}$ and $\boldsymbol{E}_{AS2}$ are given by (1) and (2), as shown at the top of the next page, where $d_1 = \Gamma_{10} + i\Delta_1$, $d_2 = \Gamma_{20} + i\Delta_2$. $\Gamma_{ij}$ is the transverse decay rate. $G_i = \mu_i E_i/\hbar$ is the Rabi frequency of the field $\boldsymbol{E}_i$. Similarly, for Λ-type three-level system, the third-order nonlinear density matrix elements of $\boldsymbol{E}_{S1}$ and $\boldsymbol{E}_{AS3}$ are given by (3) and (4), as shown at the top of the next page, where $d_3 = \Gamma_{13} + i\Delta_3$, $d_{30} = \Gamma_{03} + i(\Delta_3 - \Delta_1)$, $d_{13} = \Gamma_{13} + i\Delta_1$, $d'_{10} = \Gamma_{01} - i\Delta_3$.

When the polarization direction of pumping field $\boldsymbol{E}_1$ is modulated by a HWP, the effective density matrix elements for detected S-polarization component are given as $\rho^{(3)}_{(y)} = \rho^{(3)}_{(xxyy)} + \rho^{(3)}_{(yyyy)}$. In this case, the Rabi frequency $|G_1|^2$ in Eq. (1)-(4) is replaced by $c_x^2|G_1|^2\cos^2 2\theta$ for $\rho^{(3)}_{(xxyy)}$ and $c_y^2|G_1|^2\sin^2 2\theta$ for $\rho^{(3)}_{(yyyy)}$, respectively. When a QWP is used to change the polarization state of $\boldsymbol{E}_1$, considering different components decomposed in $x$ and y axis, together with different Clebsch-Gordan (CG) coefficients for various transitions, the Rabi frequency $|G_1|^2$ in Eq. (1)-(4) is replaced by $c_x^2|G_1^i|^2(\cos^4\theta + \sin^4\theta)$ for $\rho^{(3)}_{(xxyy)}$ and $c_y^2|G_1^i|^2\sin^2\theta\cos^2\theta$ for $\rho^{(3)}_{(yyyy)}$, respectively. Where $\theta$ is the rotated angle of the WP's axis from the $x$ axis, $c_{x,y}$ is the anisotropic factor in different direction of crystal. $G_1^i(i = -, 0, +)$ is Rabi frequency corresponding to left circular, linear and right circular polarization respectively.

### B. The Fourth–Order Fluorescence

The fourth-order FL signal is generated accompanying the FWM process with two strong pumping fields [17]. In V-type three-level system, two fluorescence signals FL1 (from $|1\rangle$ to $|0\rangle$) and FL2 (from $|2\rangle$ to $|0\rangle$) are generated simultaneously. The total intensity of fluorescence signals is the sum of two signals. Considering the coherence of the system, such process can be described by the fourth-order coherence process as shown in (5) and (6) at the top of the next page, where $d_{12} = \Gamma_{12} + i(\Delta_1 - \Delta_2)$, $d_{21} = \Gamma_{21} + i(\Delta_2 - \Delta_1)$. In Λ-type three-level system, only one fluorescence signal FL1 generated from $|1\rangle$ to $|0\rangle$, the density matrix elements of FL1 can be described by (7), as shown at the top of next page.

### C. Two Modes and Three Modes Correlation

In experiment, a pair of Stokes and anti-Stokes fields can be simultaneously created through two FWM processes. The intensity measured at Stokes and anti-Stokes channels is proportional to the third-order nonlinear density matrix elements $\rho^{(3)}_{S/AS}$. The output Stokes and anti-Stokes lights exist quantum correlation [19]. The intensity noises correlation function $G^{(2)}(\tau)$ between $\boldsymbol{E}_S$ and $\boldsymbol{E}_{AS}$ can be expressed as:

$$G^{(2)}_{S-AS}(\tau) = \frac{\left\langle (\delta\hat{I}_S(t_S))(\delta\hat{I}_{AS}(t_{AS}))\right\rangle}{\sqrt{\left\langle(\delta\hat{I}_S(t_S))^2\right\rangle\left\langle(\delta\hat{I}_{AS}(t_{AS}))^2\right\rangle}} = \frac{\left\langle Im[\delta\rho^{(3)}_S(t_S)]Im[\delta\rho^{(3)}_{AS}(t_{AS})]\right\rangle}{\sqrt{\left\langle\{Im[\delta\rho^{(3)}_S(t_S)]\}^2\right\rangle\left\langle\{Im[\delta\rho^{(3)}_{AS}(t_{AS})]\}^2\right\rangle}} \quad (8)$$

where $\tau$ is the selected time delay between Stokes and anti-Stokes signals. The correlation is positive or negative depending on the fluctuation of the imaginary part of two fields. If they have same signs, the correlation is positive. On the contrary, the correlation is negative.

$$\rho_{S1}^{(3)} = \frac{-iG_2G_{AS2}G_1}{(\Gamma_{00}+|G_2|^2/d_2+|G_1|^2/d_1)(d_2+|G_2|^2/\Gamma_{22})(d_1+|G_1|^2/\Gamma_{11})} \tag{1}$$

$$\rho_{AS2}^{(3)} = \frac{-iG_2G_{S1}G_1}{(d_2+|G_2|^2/\Gamma_{22})(d_1+|G_1|^2/\Gamma_{11})(\Gamma_{00}+|G_2|^2/d_2+|G_1|^2/d_1)} \tag{2}$$

$$\rho_{S1}^{(3)} = \frac{-iG_3G_{AS3}G_1}{(d_3+|G_3|^2/\Gamma_{11}+|G_1|^2/d_{30})(d_{13}+|G_1|^2/\Gamma_{03})(\Gamma_{03}+|G_1|^2/d_{13}+|G_3|^2/d'_{10})} \tag{3}$$

$$\rho_{AS3}^{(3)} = \frac{-iG_3G_{S1}G_1}{(d_1+|G_3|^2/d_{30}+|G_1|^2/\Gamma_{11})(d_{10}+|G_3|^2/\Gamma_{30})(\Gamma_{30}+|G_3|^2/d_{10}+|G_1|^2/d_{13})} \tag{4}$$

$$\rho_{FL1}^{(4)} = \frac{|G_2|^2}{\left(d_2+|G_2|^2/\Gamma_{00}+|G_1|^2/d_{21}\right)\left(\Gamma_{00}+|G_1|^2/d_1+|G_2|^2/d_2\right)} \times \frac{|G_1|^2}{\left(d_1+|G_1|^2/\Gamma_{00}+|G_2|^2/d_{12}\right)\left(\Gamma_{11}+|G_1|^2/d_1\right)} \tag{5}$$

$$\rho_{FL2}^{(4)} = \frac{|G_1|^2}{\left(d_1+|G_1|^2/\Gamma_{00}+|G_2|^2/d_{12}\right)\left(\Gamma_{00}+|G_1|^2/d_1+|G_2|^2/d_2\right)} \times \frac{|G_2|^2}{\left(d_2+|G_2|^2/\Gamma_{00}+|G_1|^2/d_{21}\right)\left(\Gamma_{22}+|G_2|^2/d_2\right)} \tag{6}$$

$$\rho_{11}^{(4)} = \frac{|G_1|^2}{\left(d_1+|G_1|^2/\Gamma_{11}+|G_3|^2/d_{30}\right)} \cdot \frac{|G_3|^2}{\left(d_3+|G_3|^2/\Gamma_{11}+|G_1|^2/d_{30}\right)\left(\Gamma_{11}+|G_3|^2/d_3+|G_1|^2/d_1\right)^2} \tag{7}$$

Because the FWM and fourth-order FL signals illuminated by the same pumping fields and generated simultaneously, they are also correlated with each other. The intensity of fluorescence signals is proportional to the fourth-order density matrix element, so the correlation function between fluorescence and Stokes (or anti-Stokes) signals can be written as

$$G^{(2)}_{FL-S/AS}(\tau) = \frac{\left\langle \delta\rho^{(4)}_{FL}(t_{FL})\, Im[\delta\rho^{(3)}_{S/AS}(t_{S/AS})] \right\rangle}{\sqrt{\left\langle [\delta\rho^{(4)}_{FL}(t_4)]^2 \right\rangle \left\langle \{Im[\delta\rho^{(3)}_{S/AS}(t_{S/AS})]\}^2 \right\rangle}} \tag{9}$$

Correlation between FWM and fluorescence can also be positive or negative, depending on sign of fourth-order density matrix elements and imaginary parts of the third-order density matrix elements. When fluorescence, Stokes and anti-Stokes signals coexist, we extend the two-mode correlation function $G^{(2)}(\tau)$ to the three-mode correlation function as

$$G^{(3)}_{S-AS-FL}(\tau) = \frac{\left\langle (\delta\hat{I}_S(t_S))(\delta\hat{I}_{AS}(t_{AS}))(\delta\hat{I}_{FL}(t_{FL})) \right\rangle}{\sqrt{\left\langle (\delta\hat{I}_S(t_S))^2 \right\rangle \left\langle (\delta\hat{I}_{AS}(t_{AS}))^2 \right\rangle \left\langle (\delta\hat{I}_{FL}(t_{FL}))^2 \right\rangle}} \tag{10}$$

## IV. Results and Discussion

First, we focus on the intensity evolution of FL and FWM signals at different detected time. Figures 1(e) is the pure Stokes signal detected by D1. One can see the intensity of Stokes signal decrease as the boxcar integrator gate delay. The reason is that the population decreases as the boxcar integrator gate moves backward along the time axis. Figures 1(d) show composite signals detected by D3 with very strong pumping field. In this case, there exists competition between FL and SP-FWM [17]. On the left peak in the time domain, FL is suppressed by the dressing effect, SP-FWM signal shows a sharp peak and the intensity decreases quickly with delay time. At the rising edge of the right peak in the time domain, there exists an adiabatic population transition between the dark states $|G_{2+\pm}\rangle$, so the FL signal presents AT-splitting due to the dressing effect of $\boldsymbol{E}_1$ ($|G_1|^2/d_1$ in eq. (5)), as shown at the top of this page. Finally, at the delay stage, the FL signal is from the state $|\text{-}\rangle$ spontaneous radiation, the spectra of FL signals show Lorentzian lineshapes.

Now, we investigate the correlation in $\Lambda$-type level system. In this case, the ground state coherence is induced by $\boldsymbol{E}_1$ and $\boldsymbol{E}_3$. Therefore, the Stokes and anti-Stokes signals are correlated. Figure 2(a) is the correlation function $G^{(2)}(\tau)$ between Stokes and anti-Stokes signals detected by D1 and D2 at different time positions and processed by Eq. (8). There exists strong correlation at zero delay stage. With the boxcar integrator gate delay, the magnitudes of the correlation peak $G^{(2)}(0)$ decrease as FWM signal intensity decreases in Fig. 1(e). Moreover, the values of correlation are positive. It indicates the detected intensity fluctuations of Stokes and anti-Stokes signals have same signs.

In current system, the fourth-order fluorescence FL1 is generated accompanying the FWM process, figure 2(b) and (c) show the correlations between composite signal and Stokes or anti-Stokes signal, respectively. At the left peak in the time domain, SP-FWM signal is dominant in composite signal detected by D3, hence we can see positive correlation peaks in both fig. 2(b) and (c). Gradually, correlation peak decreases with the integrator gate delay. Further increasing the delay time, FWM signal vanishes in composite signal, dominant FL signal appears the right peak (as shown in Fig.1) caused by the phonon-assisted nonradioactive transition. So we can observe correlation between pure FL1 signal and Stokes (anti-Stokes) signal at the right peak. Different

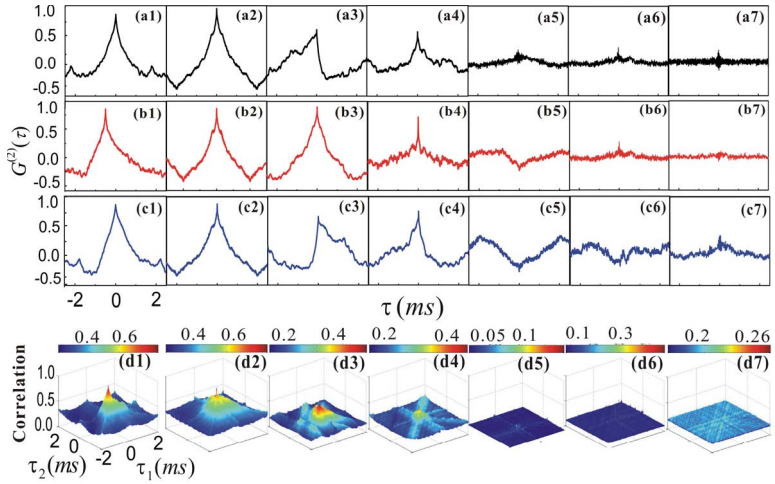


Fig. 2. (a) The two-mode correlation function $G^{(2)}(\tau)$ between $\boldsymbol{E_S}$ and $\boldsymbol{E_{AS}}$ signals (b) $\boldsymbol{E_S}$ and FL signals (c) $\boldsymbol{E_{AS}}$ and FL signals at different delay times (signed by 1 to 7 in fig. 1(c)) in Λ-type level system. (d) Three-mode correlation function $G^{(3)}(\tau)$ of $\boldsymbol{E_S}$, $\boldsymbol{E_{AS}}$ and FL signals.

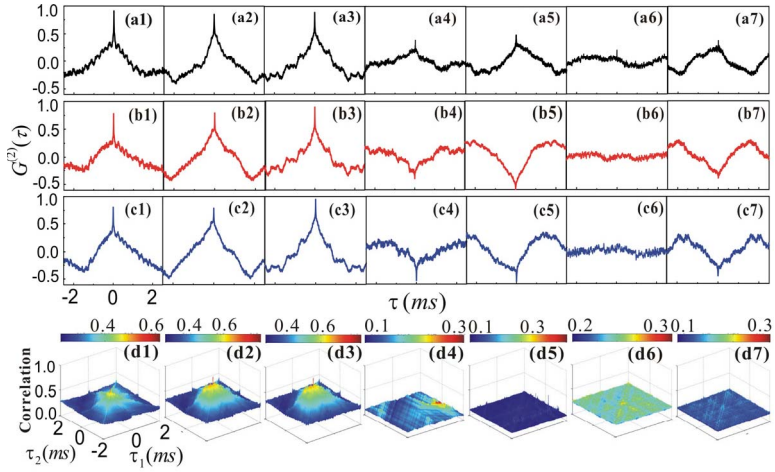


Fig. 3. (a) The two-mode correlation function $G^{(2)}(\tau)$ between $\boldsymbol{E_S}$ and $\boldsymbol{E_{AS}}$ signals (b) $\boldsymbol{E_S}$ and FL signals (c) $\boldsymbol{E_{AS}}$ and FL signals at different delay time (signed by 1 to 7 in fig. 1(c)) in V-type level system. (d) Three-mode correlation function $G^{(3)}(\tau)$ of $\boldsymbol{E_S}$, $\boldsymbol{E_{AS}}$ and FL signals.

from the correlation of FWM, FL1 and $\boldsymbol{E_S}$ ($\boldsymbol{E_{AS}}$) signals show anti-correlations. Such change can be attributed to the dressing effect and the phase fluctuations induced by phonon. As shown in Fig. 1(d), FL1 signal exhibits a suppression dip at the rising edge of the right peak due to the dressing effect of $\boldsymbol{E}_1$. Therefore, the fluctuations $\delta\rho^{(4)}_{FL}(t_{FL})$ and $Im[\delta\rho^{(3)}_{S/AS}(t_{S/AS})]$ in Eq. (9) have different signs.

Figure 2(d) show three-mode correlation function $G^{(3)}(\tau)$ of $\boldsymbol{E_S}$, $\boldsymbol{E_{AS}}$ and FL signals detected by D1, D2 and D3 and processed by Eq. (10). At the left peak, we can also see positive correlation peak of triple-beam. Comparing the correlation of three-mode with that of two-mode, one can find that the correlation level of three-mode is weaker than the case of two-mode, since the correlation condition is more stringent in three-mode. At the rising edge of the right peak in the time domain, the correlation level becomes worse because there are anti-correlations in two-mode.

Figure 3 shows correlation functions in the V-type three-level system. The values of $G^{(2)}(0)$ between Stokes and anti-Stokes signals (Fig.3 (a)) are positive and decrease with the integrator gate delay. For Stokes and FL signals in Fig.3 (b), with time position changing from left to right peak, the correlation $G^{(2)}(0)$ switches from positive to negative. Specially, the anti-correlation effect is more obvious in V-type system than in Λ-type system. It is because that there are two fluorescence signals FL1 and FL2 coexisting in V-type system. The total intensity of fluorescence signals is larger than that of Λ-type system. The correlation behavior between anti-Stokes and FL signals (Fig.3 (c)) is as same as that of Stokes and FL signals. Figure 3(d) is three-mode correlation function $G^{(3)}(\tau)$ among Stokes, anti-Stokes and FL signals. The correlation of three-mode in V-type system have similar behaviors as which in the Λ-type system.

Next, we fix the boxcar integrator gate at the left peak and change the polarization direction of $\boldsymbol{E}_1$ by HWP. Figure 4(a) shows the polarization dependence of $G^{(2)}(\tau)$ between $\boldsymbol{E_S}$ and $\boldsymbol{E_{AS}}$ signals in Λ-type level system. With the polarization direction of $\boldsymbol{E}_1$ changing from horizontal to vertical polarization ($\theta$ from 0° to 45°), one can see the correlation value $G^{(2)}(0)$ at $\tau = 0$ decreases firstly,

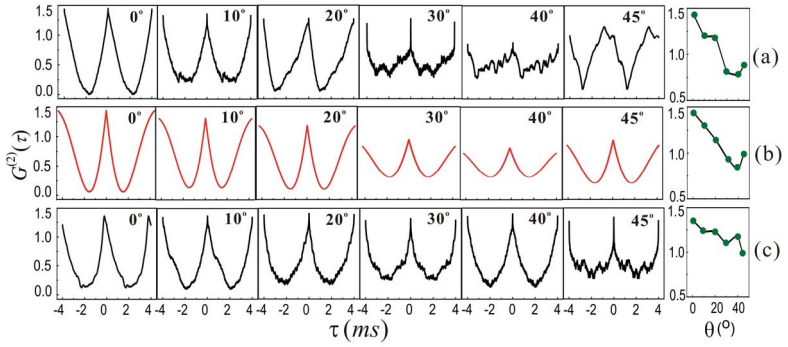


Fig. 4. Polarization dependence of $G^{(2)}(\tau)$ between $\boldsymbol{E}_{\mathbf{S}}$ and $\boldsymbol{E}_{\mathbf{AS}}$ signals and the corresponding correlation value $G^{(2)}(0)$ when the polarization direction of $\boldsymbol{E}_1$ is changed by HWP (a) experimental data in Λ-type level system, (b) Corresponding theoretical predictions of (a), (c) in V-type level system.

and then increases slightly at 45°. This phenomenon can be interpreted by the competition between gain-effect and self-dressing effect of $E_1$. The intensity noise of FWM signal is proportional to the fluctuation of the third-order nonlinear density matrix elements $\rho^{(3)}_{S/AS}$. With $\theta$ changing from 0° to 45°, the generating-terms of $\boldsymbol{E}_1$ in Eq. (3) and (4) change from $c_x^2|G_1|^2$ to $c_y^2|G_1|^2$, correlation becomes worse and worse with the decreasing of gain-effect. On the other hand, the self-dressing term $c_x^2|G_1|^2\cos^2 2\theta/d_1$ for $\rho^{(3)}_{(xxyy)}$ and $c_y^2|G_1|^2\sin^2 2\theta/d_1$ for $\rho^{(3)}_{(yyyy)}$ also decrease with $\theta$, the correlation value increases slightly at 45° because the suppression effect of $\boldsymbol{E}_1$ becomes weakest. Figure 4(b) gives the corresponding theoretical predictions by Eq. (3), (4) and (11), which agree well with the experiment results. Figure 4(c) is the polarization dependence of $G^{(2)}(\tau)$ in V-type level system. Comparing with Λ-type system, correlation peaks of V-type level system decrease slowly with $\theta$ till 45°, unlike that in Λ-type system. This indicates that the polarization dependence and the self-dressing effect of polarized state in heteronuclear-like system are weaker than homonuclear-like system.

Finally, we compare the polarization dependence of correlation at different time position. The polarization state of $\boldsymbol{E}_1$ is changed by QWP, while $\boldsymbol{E}_{2,3}$ are kept linearly polarized state. Polarized light can be decomposed into left and right circularly polarized components. In this case, the asymmetry between the right circularly and left circularly polarized components, which are defined by the polarization state of light, leads to different EIT subsystem in multi-Zeeman-level systems [20]. The correlation is governed by the EIT condition [4]. Moreover, the Clebsch-Gordan (CG) coefficients for various transitions between Zeeman sublevels are also different. Taking these two contributions into account, the intensity fluctuation and correlation of FWM and FL signals will depend sensitively on the polarization state of pumping field.

Figure 5 (a)-(c) give the correlation functions of $\boldsymbol{E}_{\mathbf{S}}$-$\boldsymbol{E}_{\mathbf{AS}}$, $\boldsymbol{E}_{\mathbf{S}}$-FL and $\boldsymbol{E}_{\mathbf{AS}}$-FL in Λ-type level system, respectively, when the boxcar integrator gate is set at the left peak. Now, SP-FWM signal is dominant in composite signal, so all correlation functions are positive. When two pumping fields $\boldsymbol{E}_1$ and $\boldsymbol{E}_3$ are linearly polarized ($\theta = 0°$), the two circularly polarized components are symmetric for realizing EIT, the maximum correlation between $\boldsymbol{E}_{\mathbf{S}}$ and $\boldsymbol{E}_{\mathbf{AS}}$ is obtained under EIT condition. When the polarization state of pumping field $\boldsymbol{E}_1$ changes to

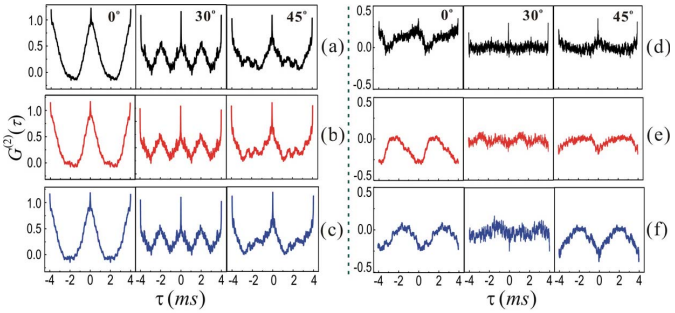


Fig. 5. Polarization dependence of $G^{(2)}(\tau)$ in Λ-type level system when the polarization states of $\boldsymbol{E}_1$ are changed by QWP. (a)-(c) $G^{(2)}(\tau)$ of $\boldsymbol{E}_{\mathbf{S}}$-$\boldsymbol{E}_{\mathbf{AS}}$, $\boldsymbol{E}_{\mathbf{S}}$-FL and $\boldsymbol{E}_{\mathbf{AS}}$-FL, respectively, when the boxcar integrator gate sets at the left peak. (d)-(e) same as (a)-(c) respectively, but the boxcar integrator gate sets at the right peak.

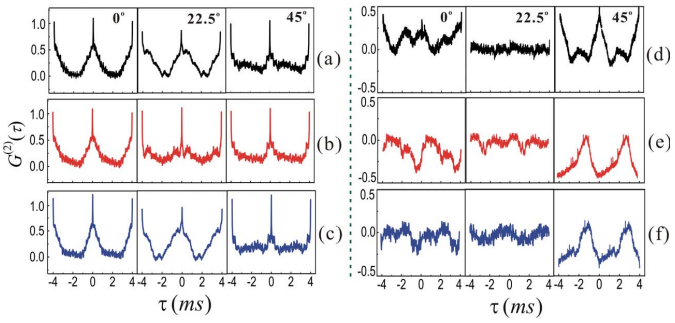


Fig. 6. Polarization dependence of $G^{(2)}(\tau)$ in V-type level system when the polarization states of $\boldsymbol{E}_1$ is changed by QWP. (a)-(c) $G^{(2)}(\tau)$ of $\boldsymbol{E}_{\mathbf{S}}$-$\boldsymbol{E}_{\mathbf{AS}}$, $\boldsymbol{E}_{\mathbf{S}}$-FL and $\boldsymbol{E}_{\mathbf{AS}}$-FL, respectively, when the boxcar integrator gate sets at the left peak. (d)-(e) same as (a)-(c) respectively, but the boxcar integrator gate sets at the right peak.

right circularly polarized ($\theta = 45°$), EIT subsystem becomes asymmetric, simultaneously, Rabi frequency changes from $c_x^2 G_2^0$ to $c_x^2 G_3^+/2$ ($c_y^2 G_3^+/2$) for $\rho^{(3)}_{(xxyy)}$ ($\rho^{(3)}_{(yyyy)}$) in Eq. (3) and (4), then the correlation of $\boldsymbol{E}_{\mathbf{S}}$-$\boldsymbol{E}_{\mathbf{AS}}$ decreases. One can see the minimum value of $G^{(2)}(0)$ appears at elliptically polarized state of $\boldsymbol{E}_1$. Moreover, correlation curve presents obviously Rabi oscillation. The correlations of $\boldsymbol{E}_{\mathbf{S}}$-FL and $\boldsymbol{E}_{\mathbf{AS}}$-FL have the same behavior with the correlation of $\boldsymbol{E}_{\mathbf{S}}$-$\boldsymbol{E}_{\mathbf{AS}}$.

Figure 5 (d)-(f) show the correlation function of $\boldsymbol{E}_{\mathbf{S}}$-$\boldsymbol{E}_{\mathbf{AS}}$, $\boldsymbol{E}_{\mathbf{S}}$-FL and $\boldsymbol{E}_{\mathbf{AS}}$-FL in Λ-type level system, respectively, when

the boxcar integrator gate sets at the right peak. The correlation of $\boldsymbol{E_S}$-$\boldsymbol{E_{AS}}$ at right peak has the same variation tendency as left peak, but $G^{(2)}(0)$ is smaller than the data at left peak due to decreasing intensity of FWM with delay time. For $\boldsymbol{E_S}$-FL and $\boldsymbol{E_{AS}}$-FL, one can see obviously anti-correlation effect in linearly and right circularly polarized states. It is because the fluorescence is dominant in composite signal at the right peak. Moreover, because of the competition of gain-effect and dressing-effect of $\boldsymbol{E}_1$, the value $G^{(2)}(0)$ is almost equal to zero at elliptically polarized state.

Figure 6 shows the polarization dependence of correlation in V-type three-level system. For results detected at left peak, all values of correlation are positive, but the variation of $G^{(2)}(0)$ with polarization is not as remarkable as in $\Lambda$-type level system. For the data detected at right peak (Fig. 6(d-f)), the polarization dependence in V-type system is in accordance with that of $\Lambda$-type system.

## V. Conclusion

In summary, we demonstrate the variation of two-mode and three-mode correlation with delay time of fluorescence and polarization states of pumping field. The correlation value $G^{(2)}(0)$ between FWM and composite signal switches from correlation to anti-correlation with delay time due to competition between SP-FWM and FL in fluorescence channel. By changing of the polarization state, all correlation curves among Stokes, anti-Stokes and fluorescence show obvious variations. Polarization control is a convenient method in practical applications. Our results provide an effective way to control correlation of multiple fields. Such multiple field correlation has variety of applications in multi-channel quantum communications and 3D quantum imaging.

## References


[1] R. H. Brown and R. Q. Twiss, "Correlation between photons in two coherent beams of light," *Nature*, vol. 177, no. 4497, pp. 27–29, 1956.

[2] F. Wang, I. Toselli, J. Li, and O. Korotkova, "Measuring anisotropy ellipse of atmospheric turbulence by intensity correlations of laser light," *Opt. Lett.*, vol. 42, no. 6, pp. 1129–1132, 2017.

[3] M. D. Lukin, A. B. Matsko, M. Fleischhauer, and M. O. Scully, "Quantum noise and correlations in resonantly enhanced wave mixing based on atomic coherence," *Phys. Rev. Lett.*, vol. 82, pp. 1847–1850, Mar. 1999.

[4] V. A. Sautenkov, Y. V. Rostovtsev, and M. O. Scully, "Switching between photon-photon correlations and Raman anticorrelations in a coherently prepared Rb vapor," *Phys. Rev. A, Gen. Phys.*, vol. 72, no. 6, Dec. 2005, Art. no. 065801.

[5] X. H. Yang, J. T. Sheng, U. Khadka, and M. Xiao, "Generation of correlated and anticorrelated multiple fields via atomic spin coherence," *Phys. Rev. A, Gen. Phys.*, vol. 85, no. 1, 2012, Art. no. 013824.

[6] H. J. Kimble, M. Dagenais, and L. Mandel, "Photon antibunching in resonance fluorescence," *Phys. Rev. Lett.*, vol. 39, no. 11, pp. 691–695, 1977.

[7] Z. Qin, L. Cao, H. Wang, A. M. Marino, W. Zhang, and J. Jing, "Experimental generation of multiple quantum correlated beams from hot rubidium vapor," *Phys. Rev. Lett.*, vol. 113, Jul. 2014, Art. no. 023602.

[8] X. Jia *et al.*, "Experimental realization of three-color entanglement at optical fiber communication and atomic storage wavelengths," *Phys. Rev. Lett.*, vol. 109, Dec. 2012, Art. no. 253604.

[9] J. Li and F. Chen, "Correlation between intensity fluctuations of light generated by scattering of Young's diffractive electromagnetic waves by a quasi-homogeneous, anisotropic medium," *Laser Phys. Lett.*, vol. 13, no. 11, Oct. 2016, Art. no. 116004.

[10] J. Li, F. Chen, and L. Chang, "Correlation between intensity fluctuations of electromagnetic waves scattered from a spatially quasi-homogeneous, anisotropic medium," *Opt. Exp.*, vol. 24, no. 21, pp. 24274–24286, 2016.

[11] J. Li, Y. Qin, and S. Zhou, "Fourth-order correlation statistics of an electromagnetic plane wave scattered by a quasi-homogeneous medium," *J. Opt.*, vol. 13, no. 11, 2011, Art. no. 115702.

[12] B. S. Ham, P. R. Hemmer, and M. S. Shahriar, "Efficient electromagnetically induced transparency in a rare-earth doped crystal," *Opt. Commun.*, vol. 144, nos. 4–6, pp. 227–230, 1997.

[13] H.-H. Wang *et al.*, "Enhanced four-wave mixing by atomic coherence in a $Pr^{3+}$:$Y_2SiO_5$ crystal," *Appl. Phys. Lett.*, vol. 93, no. 23, 2008, Art. no. 221107.

[14] J. J. Longdell, E. Fraval, M. J. Sellars, and N. B. Manson, "Stopped light with storage times greater than one second using electromagnetically induced transparency in a solid," *Phys. Rev. Lett.*, vol. 95, no. 6, 2005, Art. no. 063601.

[15] R. Wang *et al.*, "Polarization dressed multi-order fluorescence of $Pr^{3+}$:$Y_2SiO_5$," *Phys. Chem. Chem. Phys.*, vol. 16, no. 29, pp. 15623–15629, 2014.

[16] H. Zheng *et al.*, "Seeded spontaneous parametric four-wave mixing and fluorescence of $Pr^{3+}$:YSO," *Laser Phys. Lett.*, vol. 11, no. 11, 2014, Art. no. 116102.

[17] H. Lan *et al.*, "Competition between spontaneous parametric four-wave-mixing and fluorescence of $Pr^{3+}$:YSO," *Laser Phys. Lett.*, vol. 12, no. 1, 2014, Art. no. 015404.

[18] R. Wang *et al.*, "Modulating the correlation and squeezing of phase-conjugate four-wave mixing via the polarizable dressing states," *Phys. Chem. Chem. Phys.*, vol. 17, no. 20, pp. 13442–13450, 2015.

[19] H. X. Chen *et al.*, "Parametric amplification of dressed multi-wave mixing in an atomic ensemble," *Laser Phys. Lett.*, vol. 11, no. 4, 2014, Art. no. 045201.

[20] B. Wang, S. J. Li, J. Ma, H. Wang, K. C. Peng, and M. Xiao, "Controlling the polarization rotation of an optical field via asymmetry in electromagnetically induced transparency," *Phys. Rev. A, Gen. Phys.*, vol. 73, no. 5, 2006, Art. no. 051801.



**Ruimin Wang** was born in Shaanxi, China, in 1970. She received the Ph.D. degree from the School of Science, Xi'an Jiaotong University, China, in 2006. She is currently an Associate Professor with the School of Science, Xi'an Jiaotong University. Her research interests include nonlinear optics and quantum optics.

**Yang Liu** was born in Shaanxi, China, in 1991. He is currently pursuing the master's degree in optics engineering with the Xi'an Institute of Optics and Precision Mechanics, Chinese Academy of Sciences, Xi'an Jiaotong University. His research interests include optical fiber communication and quantum optics.

**Kangkang Li** was born in Shaanxi, China, 1993. He is currently pursuing the master's degree in physical electronics with Xi'an Jiaotong University, China. He is currently with the Key Laboratory of Physical Electronics and Devices, Ministry of Education, Xi'an Jiaotong University.

**Peng Li** was born in Shaanxi, China, in 1994. He is currently pursuing the master's degree with the Key Laboratory of Physical Electronics and Devices, Ministry of Education, Xi'an Jiaotong University. His research interests include functional micro/nanocrystals, nonlinear optics, and quantum optics filed.

**Muhammad Owais** was born in Kohat, Pakistan, in 1991. He received the bachelor's degree in electronics engineering from the Dawood University of Engineering and Technology, Karachi. He is currently pursuing the master's degree in electronic engineering with Xi'an Jiaotong University, China. His current research interests include nonlinear optics and quantum optics.

**Yanpeng Zhang** was born in Shaanxi, China, in 1969. He received the Ph.D. degree in electronics engineering from Xi'an Jiaotong University, China, in 2000. He is currently an Associate Professor with the Key Laboratory of Physical electronics and Devices, Ministry of Education, Xi'an Jiaotong University. His research interests are nonlinear optics and quantum optics.